Chemosphere 359 (2024) 142292

Contents lists available at ScienceDirect

Chemosphere

journal homepage: www.elsevier.com/locate/chemosphere

Synergies of chemodenitrification and denitrification in a saline inland lake

Rosanna Margalef-Marti [a,b,*], Aubin Thibault De Chanvalon [a], Pierre Anschutz [c], David Amouroux [a], Mathieu Sebilo [a,d]

[a] Université de Pau et des Pays de l'Adour, E2S UPPA, CNRS, Institut des Sciences Analytiques et de Physico-chimie pour l'Environnement et les Matériaux (IPREM), Pau, France
[b] Grup MAiMA, MAGH, Departament de Mineralogia, Petrologia i Geologia Aplicada, Facultat de Ciències de La Terra, Universitat de Barcelona (UB), 08028, Barcelona, Spain
[c] Univ. Bordeaux, CNRS, Bordeaux INP, EPOC, UMR 5805, F-33600, Pessac, France
[d] Sorbonne Université, CNRS, IEES, Paris, France

HIGHLIGHTS

- Ferrous iron in Gallocanta lake drives nitrate and nitrite reduction.
- Chemodenitrification seems enhanced by the addition of external ferrous iron.
- Chemodenitrification experiments leaded to $\varepsilon^{15}N_{NO2}$ between −6.8 and −12.3 ‰.
- Denitrification experiments leaded to $\varepsilon^{15}N_{NO3}$ between −8.5 and −15.1 ‰.

GRAPHICAL ABSTRACT

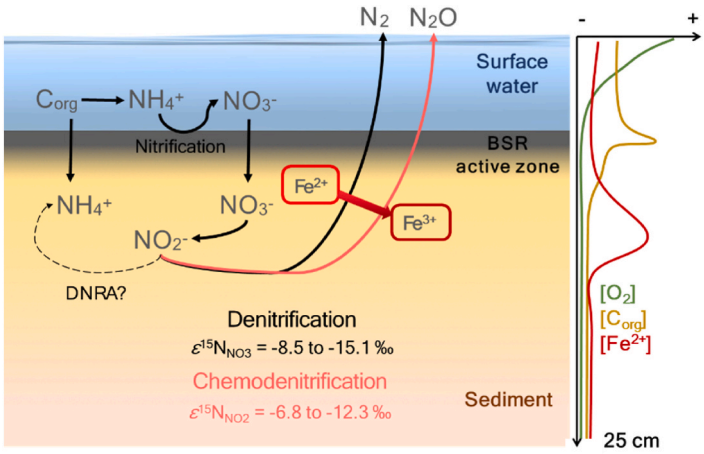

ARTICLE INFO

Handling editor: Yongmei Li

Keywords:
Chemodenitrification
Nitrogen cycling
Ferrous iron
Isotopic fractionation
Gallocanta lake

ABSTRACT

The interconnection between biotic and abiotic pathways involving the nitrogen and iron biogeochemical cycles has recently gained interest. While lacustrine ecosystems are considered prone to the biotic nitrate reduction (denitrification), their potential for promoting the abiotic nitrite reduction (chemodenitrification) remains unclear. In the present study, batch incubations were performed to assess the potential for chemodenitrification and denitrification in the saline inland lake Gallocanta. Sulfidic conditions are found in top sediments of the system while below (5–9 cm), it presents low organic carbon and high sulfate and ferrous iron availability. Anoxic incubations of sediment (5–9 cm) and water from the lake with nitrite revealed potential for chemodenitrification, especially when external ferrous iron was added. The obtained isotopic fractionation values for nitrite ($\varepsilon^{15}N_{NO2}$) were −6.8 and −12.3 ‰ and therefore, fell in the range of those previously reported for the

* Corresponding author. Grup MAiMA, MAGH, Departament de Mineralogia, Petrologia i Geologia Aplicada, Facultat de Ciències de La Terra, Universitat de Barcelona (UB), 08028, Barcelona, Spain.
E-mail address: rosannamargalef@ub.edu (R. Margalef-Marti).

https://doi.org/10.1016/j.chemosphere.2024.142292
Received 25 February 2024; Received in revised form 3 May 2024; Accepted 7 May 2024
Available online 8 May 2024

nitrite reduction. The more pronounced $\varepsilon^{15}N_{NO2}$ (−12.3 ‰) measured in the experiment containing additional ferrous iron was attributed to a higher contribution of the chemodenitrification over biotic denitrification. Incubations containing nitrate also confirmed the potential for denitrification under autotrophic conditions (low organic carbon, high ferrous iron). Higher reaction rate constants were found in the experiment containing 100 μM compared to 400 μM nitrate. The obtained $\varepsilon^{15}N_{NO3}$ values (−8.5 and −15.1 ‰) during nitrate consumption fell in the range of those expected for the denitrification. A more pronounced $\varepsilon^{15}N_{NO3}$ (−15.1 ‰) was determined in the experiment presenting a lower reaction rate constant (400 μM nitrate). Therefore, in Gallocanta lake, nitrite generated during nitrate reduction can be further reduced by both the abiotic and biotic pathways. These findings establish the significance of chemodenitrification in lacustrine systems and support further exploration in aquatic environments with different levels of C, N, S, and Fe. This might be especially useful in predicting nitrous oxide emissions in natural ecosystems.

1. Introduction

During the last decades, anthropogenic activities have boosted the exports of reactive nitrogen compounds to ecosystems, leading to water bodies eutrophication (Beusen et al., 2016; Gruber and Galloway, 2008). Some of the nitrogen cycling pathways occurring naturally in the environment can partially mitigate this deterioration such as N assimilation by plants and microorganisms or the denitrification (Knowles, 1982; Lin and Stewart, 1997; Masclaux-Daubresse et al., 2010).

The denitrification (nitrate (NO_3^-) reduction to N_2 through a series of enzyme-mediated reactions involving the intermediates nitrite (NO_2^-), nitric oxide (NO) and nitrous oxide (N_2O)), has been thoroughly studied at laboratory and field-scales (Akunna et al., 1993; Khan and Spalding, 2004; Knowles, 1982; Kraft et al., 2011; Margalef-Marti et al., 2019). It is a well-known process allowing the return of bioavailable N to the atmosphere (Hauck, 1984). In contrast, abiotic reduction processes involving NO_2^- had not gained attention until one decade ago (Coby and Picardal, 2005; Dhakal et al., 2013; Klueglein and Kappler, 2013; Rakshit et al., 2008). NO_2^- is an intermediate of several N cycling pathways, including denitrification (Knowles, 1982). Recent studies have pointed that NO_2^- can undergo abiotic reduction to N_2O through oxidation of ferrous iron (Fe^{2+}) in an anaerobic process known as chemodenitrification (CDNT) (Carlson et al., 2013; Chen et al., 2018; Coby and Picardal, 2005; Rakshit et al., 2016). Given the environmental significance of N_2O as a greenhouse gas (Badr and Probert, 1993), understanding CDNT becomes crucial to prevent pollution swapping unless N_2O is further reduced to N_2. Current knowledge on CDNT primarily stems from laboratory experiments which may not fully replicate field conditions. Thus, further research is required to determine the relevance and the specific environmental conditions under which the CDNT occurs at the ecosystem level. Compounds such as iron, sulfur, organic carbon and oxygen, known to drive the denitrification over other biotic N cycling processes in aquatic ecosystems (Burgin and Hamilton, 2007; Cojean et al., 2020), are also suspected to impact CDNT.

One of the main challenges in studying CDNT at fields-scale in aquatic ecosystems is its simultaneous occurrence with denitrification, since both reactions can be induced by Fe^{2+} oxidation, and/or with other biotic pathways. Traditional measurement of nitrogen compounds concentrations alone cannot determine the multiple processes involved due to the dual role of intermediates as products and substrates. In complement, the measurement of stable isotope ratios and associated isotopic fractionation can be a very powerful tool to discriminate among various processes and refine reaction mechanisms. In the course of the enzymatic NO_3^- reduction, the unreacted residual substrate becomes enriched in the heavy isotopes ^{15}N and ^{18}O, since the lighter isotopes (^{14}N and ^{16}O) react preferentially (Aravena and Robertson, 1998; Böttcher et al., 1990; Fukada et al., 2003; Mariotti et al., 1981). While nitrogen stable isotope data have been previously employed to trace enzymatic processes, such as the denitrification, isotopic studies on CDNT remain scarce (Abu et al., 2024; Buchwald et al., 2016; Jones et al., 2015; Liu et al., 2018). Determining the extent of isotopic fractionation (ε) during CDNT becomes critical for assessing the potential of isotopic tools to trace CDNT in ecosystems in situ.

Endorheic lakes are appropriate environments to study interactions between nutrient cycling pathways since they are uniquely influenced by geological background, nutrient loading, and meteorological conditions (Jolly et al., 2008; Williams, 2002). In the saline inland lake Gallocanta, bacterial sulfate (SO_4^{2-}) reduction (BSR) has been detected near the water-sediment interface due to high organic C content that induce anaerobic conditions as well as an active iron cycling (Castañeda et al., 2017; Corzo et al., 2005; Margalef-Marti et al., 2023). The availability of electron donors points that environmental conditions may be conducive to the occurrence of CDNT and denitrification. However, no study on N cycle has been performed in Gallocanta lake up to date. In this context, the main goal of the present study was to assess the potential occurrence of CDNT and denitrification in Gallocanta lake sediment and additionally to determine the environmental conditions inducing these processes. An integrated geochemical and isotopic approach, combining field measurements and laboratory experiments, was conducted to provide insights into biotic and abiotic N cycling pathways and their modulation by iron and sulfur content in the system.

2. Methods

2.1. In vitro nitrate and nitrite reduction experiments

Gallocanta lake, located on a plateau within the Iberian Range at 990 m a.s.l., covers a surface of 14 km^2 and exhibits saline conditions (20–40 mS/cm). The lake, characterized by a pH range between 8 and 10 (CHE, 2005), is ephemeral and hosts macrophytes (*Ruppia drepanensis*) on its bed, with a large community of migratory crane (*Grus grus*) population from November to March, leading to substantial organic matter inputs (Alonso López, J.A. et al., 1990a; Alonso López, J.C. et al., 1990b; Castañeda et al., 2020). In October 2022, water and sediment samples were collected from one selected station in Gallocanta lake (N 40°57.8499′ and W 001°30.4894′). Water was collected at a depth of 15 cm, corresponding to the middle of the water column (30 cm depth in total). After three rinses with water from the lake, a PP container was placed sealed at the specified depth and then opened to completely fill it without leaving free headspace. Sediment cores were collected in sealed PVC tubes (10 cm diameter, 40 cm height). Immediately after obtention the sediment cores were sliced inside an anaerobic chamber under a N_2 atmosphere to keep the depth intervals between the surface and 5 cm and between 5 and 9 cm while the remaining deeper sediment was discarded. The obtained water and sediment were characterized geochemically following the methodology described in (Margalef-Marti et al., 2023) and were employed to set-up batch incubations as described below.

Batch incubations were set-up immediately after sampling in 50 mL pre-combusted glass vials under anaerobic conditions. The water used for the experiments was preventively deoxygenated by purging it for 1 h with argon gas and the absence of oxygen was confirmed at the end of the purge. Glass vials containing 4 g of fresh sediment supplemented with deoxygenated water were crimp sealed with butyl rubber stoppers. According to previous results, sediment in the 0–5 cm range was rich in organic matter and sulfide (S^{-2}), while sediment at depths between 5

and 9 cm exhibited low organic C content and high availability of Fe^{2+} (details can be found in section 3.1 and in (Margalef-Marti et al., 2023)). Therefore, deep sediment (5–9 cm) exhibited conditions conducive to low heterotrophic bacterial activity and a high potential for autotrophic bacterial activity or abiotic processes involved in both nitrogen and iron cycling. A total of 6 different conditions were tested in triplicates (Table 1).

Incubations of the 6 types of experiments were conducted simultaneously, with constant shaking, in the dark, at approximately 20 °C. The bottles were sacrificed at sequential time based on NO_2^- accumulation and reduction dynamics. Water samples from sacrificed flasks were immediately filtered through 0.2 μm syringe filters and conditioned as follows. Aliquots for NO_3^-, NO_2^- and NH_4^+ concentration and isotopic composition determination were frozen at −20 °C. A zinc acetate solution (20 g/L) was added to aliquots for sulfide concentration determination. A ferrozine solution was added to aliquots for total Fe and Fe^{2+} measurements.

2.2. Analytical methods

Concentrations of NO_3^-, NO_2^-, NH_4^+, Fe^{2+}, Fe^{3+} and $\sum S^{2-}$ (H_2S, HS^- and S^{2-}) were determined by spectrophotometry using specific methods based on the formation of colored complexes with an intensity proportional to the reagent concentration. The NO_3^- was reduced to NO_2^- with a vanadium chloride solution and then NO_2^- formed a pink complex by reacting with sulfanilamide and N-Naphtyl-1-éthylènediamine solutions in acidic media, then absorbance was read at 543 nm wavelength (García-Robledo et al., 2014). The NO_2^- was measured following the second step of the aforementioned reaction. The NH_4^+ formed a blue complex by reacting with dichlorocyanuric acid and phenol in the presence of nitroprussiate and in basic medium, then absorbance was read at 630 nm (Koroleff, 1976). The Fe^{2+} formed a violet complex by reacting with ferrozine in ammonium acetate buffer (0.5 M), then absorbance was read at 562 nm after 24 h (Greenberg et al., 1992; Stookey, 1970). For total Fe (Fe^{2+} + Fe^{3+}) determination, 1 M HCl and ascorbic acid (50 mM final concentration) were added to reduce Fe^{3+} to Fe^{2+} and then the aforementioned method was applied. The $\sum S^{2-}$ concentration was determined after precipitation as ZnS (described in section 2.1) which forms a blue complex in the presence of diamine and iron chloride, then absorbance is read at 660 nm (Fonselius, 1983). Minisensor probes (unisense) were employed to determine qualitative N_2O content after daily calibration. The isotopic composition of dissolved N compounds ($\delta^{15}N$–NH_4^+, $\delta^{15}N$–NO_3^-, $\delta^{18}O$–NO_3^-, $\delta^{15}N$–NO_2^- and $\delta^{18}O$–NO_2^-) have been determined after their subsequent chemical transformation into NO_2^- and N_2O. Dissolved NH_4^+ was oxidized to NO_2^- by using a hypobromite solution (Zhang et al., 2007). Dissolved NO_3^- was reduced to NO_2^- using spongy cadmium (McIlvin and Altabet, 2005; Ryabenko et al., 2009). Then, for all the samples, NO_2^- was reduced to N_2O with a sodium azide solution with acetic acid (McIlvin and Altabet, 2005; Ryabenko et al., 2009; Zhang et al., 2007). Simultaneous $\delta^{15}N$ and $\delta^{18}O$ analysis of N_2O produced during the conversion of NH_4^+, NO_3^- and NO_2^- was carried out using a Pre-Con (Thermo Scientific) coupled to a Finnigan MAT-253 Isotope Ratio Mass Spectrometer (IRMS, Thermo Scientific). The standard deviation reproducibility of the samples was ±1.0 ‰ for $\delta^{15}N$ of dissolved NO_3^-, NO_2^- and NH_4^+ and ±1.5 ‰ for $\delta^{18}O$ of dissolved NO_3^- and NO_2^-. The isotopic notation is expressed in terms of δ per mil relative to international standards Atmospheric N_2 (AIR) for $\delta^{15}N$ and Vienna Standard Mean Oceanic Water (VSMOW) for $\delta^{18}O$, following:

$$\delta = \frac{R_{sample} - R_{standard}}{R_{standard}}, \text{ where } R = {}^{15}N/{}^{14}N \text{ and } {}^{18}O/{}^{16}O, \text{ respectively.}$$

Table 1
Tested conditions in batch experiments. In the chemodenitrification experiments, deionized water was used instead of the lake water to reduce bacterial activity. In the case of external compounds addition, NO_3^- was added as KNO_3, NO_2^- was added as $NaNO_2$ and Fe^{2+} was added as $FeSO_4$.

Process involved	Code	Sediment depth (4 g)	Water type (50 mL)	Added compounds
Ammonification – surface Control experiment to determine possible natural N compounds release and transformation from surface sediment (heterotrophic)	sAMON	0–5	Lake	x
Ammonification Control experiment to determine possible natural N compounds release and transformation from deep sediment (autotrophic)	AMON	5–9	Lake	x
Denitrification – higher NO_3^- Experiment to test the potential of denitrification and/or DNRA in deep sediment (autotrophic)	hDNT	5–9	Lake	NO_3^- 400 μM
Denitrification – lower NO_3^- Experiment to test the potential of denitrification and/or DNRA in deep sediment (autotrophic)	lDNT	5–9	Lake	NO_3^- 100 μM
Chemodenitrification – lower Fe^{2+} Experiment to test the potential of chemodenitrification and/or biotic NO_2^- reduction in deep sediment (autotrophic)	CHDN	5–9	mQ	NO_2^- 500 μM
Chemodenitrification – higher Fe^{2+} Experiment to test the potential of chemodenitrification and/or biotic NO_2^- reduction in deep sediment (autotrophic)	FeCHD	5–9	mQ	NO_2^- 500 μM Fe^{2+} 500 μM

2.3. Isotopic fractionation calculation

Under closed system conditions, with no substrate renewal, in the absence of isotopic exchange and considering a unidirectional irreversible reaction, the isotopic fractionation (ε) of NO_3^- and NO_2^- can be calculated by means of the Rayleigh distillation type equation (Böttcher et al., 1990; Denk et al., 2017; Mariotti et al., 1988):

$$\delta_{residual} = \delta_{initial} + \varepsilon \ ln\left(\frac{C_{residual}}{C_{initial}}\right)$$

Thus, ε can be obtained from the slope of the linear correlation between the natural logarithm of the substrate remaining fraction (C refers to the analyte concentration) and the determined isotopic composition.

3. Results and discussion

3.1. Nitrogen and iron in porewater from gallocanta lake

The main geochemical characteristics of surface water and porewater in Gallocanta lake are summarized in the Supporting Information S1. Since Fe and N compounds are involved in the reactivity of batch incubations, here we briefly described its measured content in Gallocanta Lake porewater during the October 2022 campaign. Also, we compared these findings with the results obtained for previous campaigns performed in November 2020 and June 2021 (Margalef-Marti et al., 2023).

Porewater from Gallocanta Lake exhibited Fe concentrations of up to 150 μM (Fig. 1A to C). A marked peak on Fe concentrations was observed approximately at the middle of the sediment cores, with depths

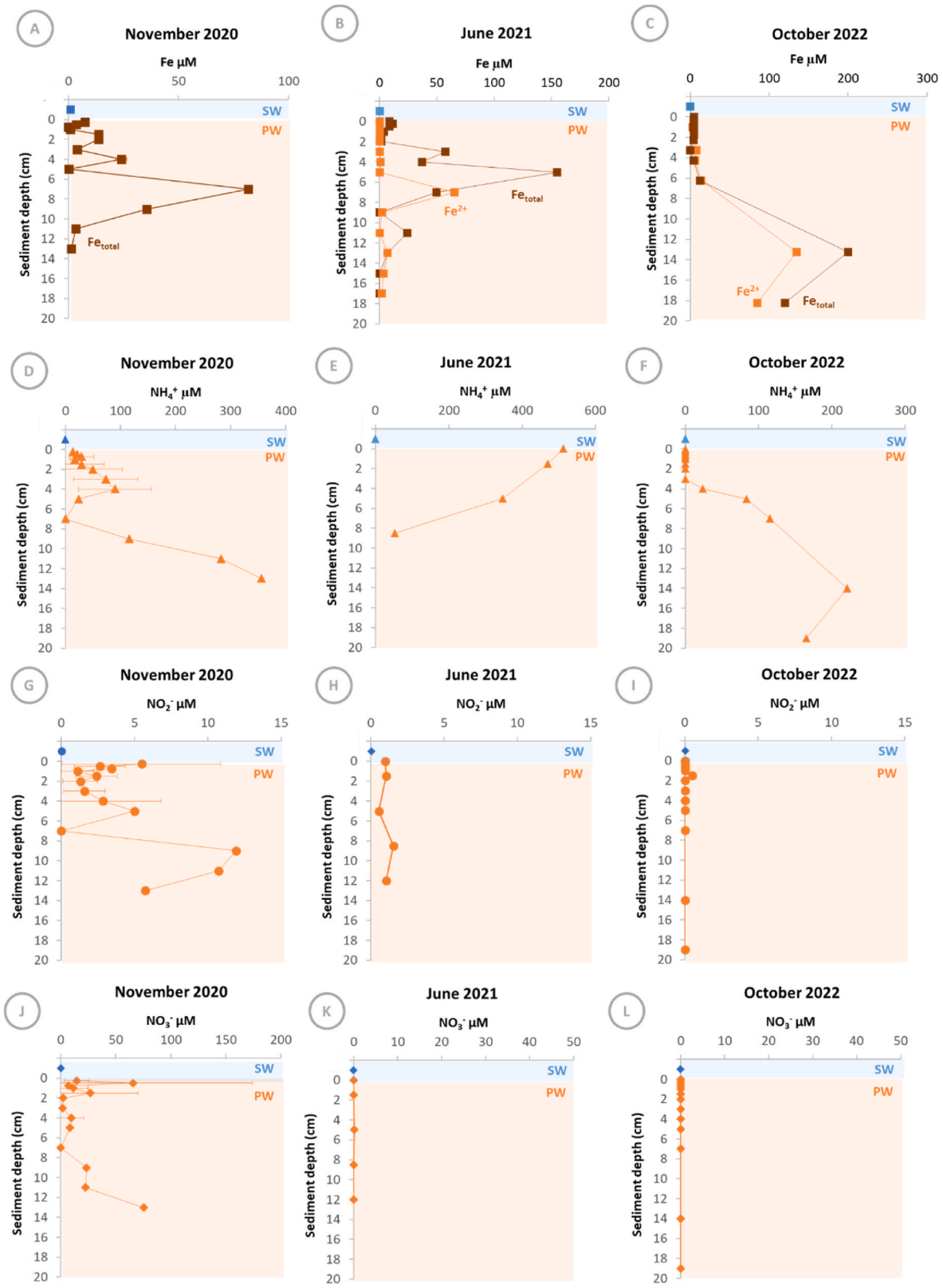

Fig. 1. Iron and nitrogen compounds in porewater from Gallocanta lake. Dissolved Fe (A, B, C), ammonium (D, E, F), nitrite (G, H, I) and nitrate (J, K, L) concentrations measured in porewater in November 2020, June 2021 and October 2022. Error bars in the November 2020 plots reflects the standard deviation from averages calculated for three different cores. Fe^{2+} was not measured in November 2020. SW = surface water (blue), PW = porewater (orange). (For interpretation of the references to color in this figure legend, the reader is referred to the Web version of this article.)

varying between 4 and 13 cm in different campaigns. Iron speciation analysis highlighted that a substantial portion existed as Fe^{2+}, reinforcing the potential for NO_3^- dependent iron oxidation and CDNT at this depth. Another pool of labile iron was identified in the solid fraction (sediment) through the acid volatile sulfide (AVS) extraction (1 M HCl) which allows quantitative extraction of mackinawite (Rickard and Morse, 2005). AVS shows very high content (up to 3700 μmol g^{-1}) associated with high $\sum S^{2-}$ concentration (up to 1100 μM), in the BSR active zone (Supporting Information S2). This points that iron sulfides and S^{2-} could only play a role on denitrification in surface sediment, where organic C is also available. The availability of Fe^{2+} for microbial oxidation can also be enhanced by the presence of ligands (Zhao et al., 2020).

Regarding N compounds, porewater contained NH_4^+ levels up to 500 μM (Fig. 1D to F). Moreover, NO_3^- and NO_2^- were detected in porewater but only in the first of the 3 campaigns, with concentrations reaching up to 65 and 12 μM, respectively Fig. 1G to L). The depth profile of N compounds content exhibited variations across campaigns, suggesting an active N cycling. A detailed discussion on the potential N sources to the system is provided in Supporting Information S3 and S4.

3.2. Nitrogen compounds reactivity in sediment from gallocanta lake

When incubating surface sediment with water from the lake (0–5 cm depth, sAMON), no NH_4^+, NO_3^-, or NO_2^- were released from sediment (Fig. 2A). In contrast, when incubating deep sediment (5–9 cm depth, AMON) resulted in the rapid release of up to 5 μM NH_4^+ (Fig. 2B). These results supported field observations since NH_4^+ was below detection limit in porewater from the top 3 cm of sediment while the highest concentrations were measured at 7 cm depth in October 2022 (125 μM, Fig. 1F). The $\sum S^{2-}$ concentrations increased over time in the sAMON experiment reaching up to 130 μM (Fig. 2C), and confirming the availability of organic matter for BSR and mineralization. The absence of simultaneous accumulation of dissolved NH_4^+ in the sAMON experiment could be attributed to adsorption and/or volatilization under alkaline conditions (pH = 9.0–9.5) (Hargreaves, 1998). In contrast, and as expected, S^{2-} was not detected in the AMON experiment due to the much lower organic content compared to sAMON (Fig. 2D). Indeed, the measured 5 μM NH_4^+ was the concentration expected from diluting deep sediment porewater (4 g, 125 μM NH_4^+) with surface water (45 mL, no NH_4^+). This suggested a lack of a significant mineralization activity in deep sediment and reinforced that different N cycling pathways take place in deep compared to surface sediment.

Concerning Fe, no release was observed in the sAMON experiment while up to 11 μM accumulated in AMON from ~3000 min onwards (Fig. 2C and D). This is consistent with field observations, as lower dissolved Fe concentrations were measured in surface sediment compared to deep sediment (Fig. 1C), and confirms a higher Fe reactivity in deep sediment. The lower Fe content in surface sediment is likely due to its precipitation with the S^{2-} produced from the high BSR activity.

The potential for denitrification and/or dissimilatory NO_3^- reduction to NH_4^+ (DNRA) was tested in the lDNT and hDNT experiments, which involved deep sediment and NO_3^- at concentrations of 100 or 400 μM, respectively. In lDNT (Fig. 3A), a lag-time of ~700 min was observed before the decrease of NO_3^- concentration, which lasted for more than

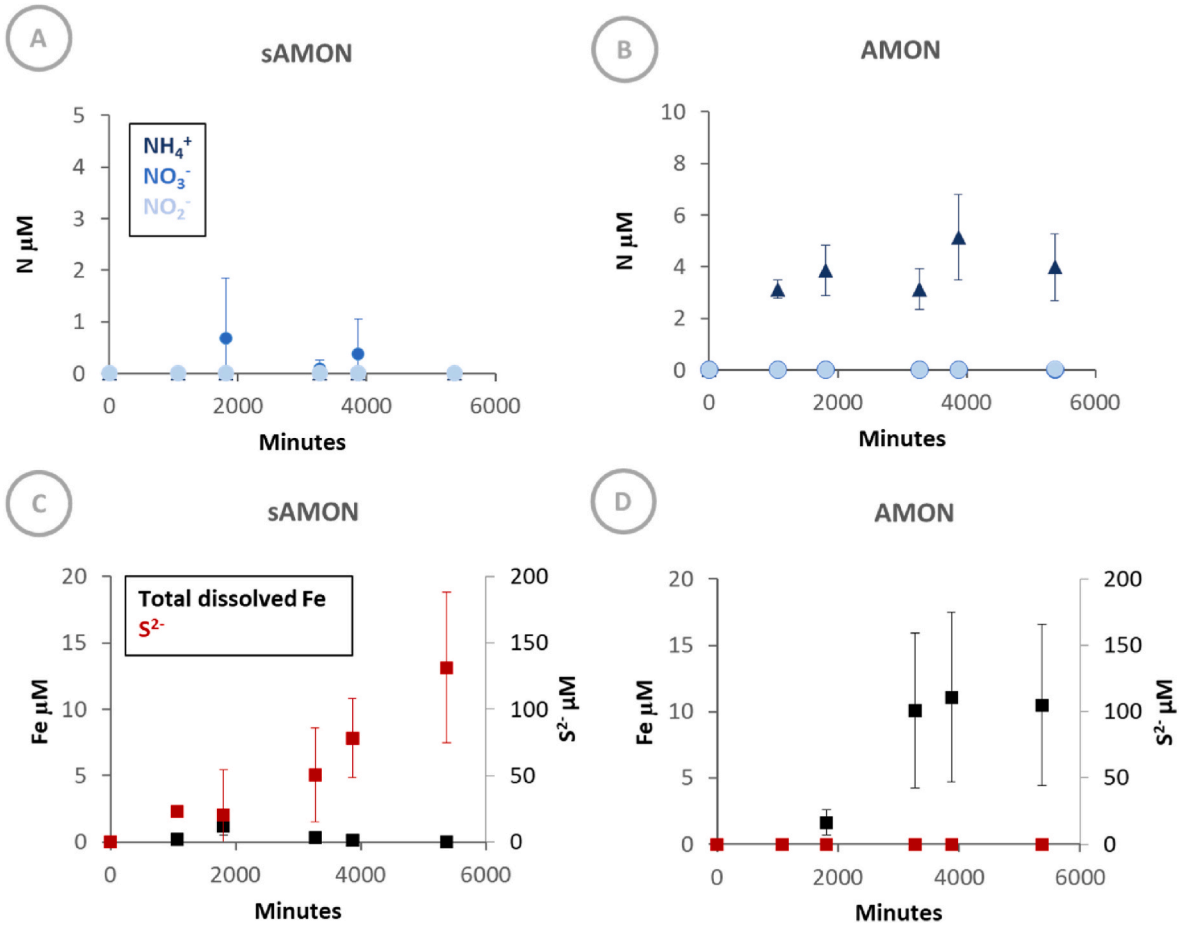

Fig. 2. Ammonification experiments results. Plots A and B show the measured concentration of ammonium (dark blue triangles), nitrate (blue rhombus) and nitrite (light blue circle), while plots C and D show the measured concentration of sulphide (red squares) and total dissolved iron (black squares). (For interpretation of the references to color in this figure legend, the reader is referred to the Web version of this article.)

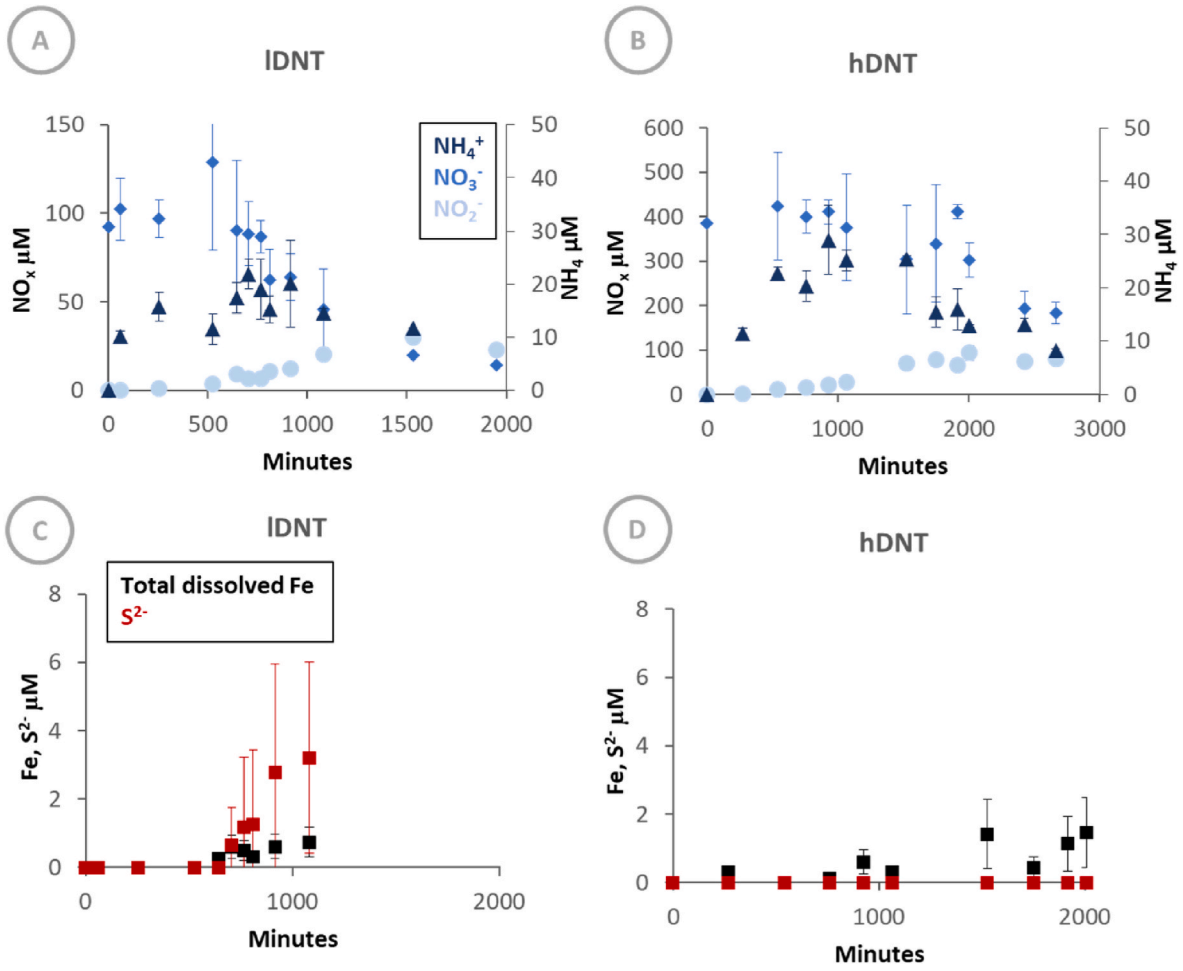

Fig. 3. Denitrification experiments results. Plots A and B show the measured concentration of ammonium (dark blue triangles), nitrate (blue rhombus) and nitrite (light blue circle), while plots C and D show the measured concentration of sulphide (red squares) and total dissolved iron (black squares). (For interpretation of the references to color in this figure legend, the reader is referred to the Web version of this article.)

2000 min. During the lag-time, NH_4^+ accumulated up to 25 μM then decreased simultaneously with NO_3^-. Conversely, NO_2^- accumulated only during the period of NO_3^- reduction reaching up to 30 μM. A similar pattern was observed in hDNT (Fig. 3B), with a lag-time of ~1000 min characterized by NH_4^+ accumulation (up to 29 μM) followed by NO_3^- reduction period lasting for more than 2700 min, accompanied by NH_4^+ consumption and NO_2^- build up (to 94 μM).

The lag-time observed before the NO_3^- concentration decrease suggested that denitrifying microorganisms in the sediment were inactive state during the sampling period. This is consistent with the non-detection of NO_3^- or NO_2^- in field porewater samples in October 2022 (Fig. 1I and L). Concerning intermediate products accumulation, the measured NO_2^- corresponded to up to 30 % and 20 % of the initial NO_3^--N in lDNT and hDNT, respectively. Transient NO_2^- accumulation is usually observed in denitrification experiments since NO_2^- reductases are activated later than NO_3^- reductases (Zumft, 1997). Regarding NH_4^+, its accumulation began before the start of NO_3^- reduction in both experiments, and the measured concentration (25–29 μM) was higher than the content measured in the AMON experiment (5 μM). Since NH_4^+ concentration increased while NO_3^- concentration remained stable, it is unlikely that DNRA played a major role on NH_4^+ release. Remineralisation or sediment desorption could be alternative sources of NH_4^+. The later hypothesis was likely in accordance with the isotopic characterization of NH_4^+ and a detailed discussion is provided in Supporting information S5. The decrease of NH_4^+ concentration by the end of the experiments might be explained by a possible readsorption on sediment or by anammox.

The NO_3^- reduction period occurred simultaneously to the release of reduced dissolved species (iron and sulfur), suggesting NO_3^- reduction dependent on Fe^{2+} oxidation, i.e., autotrophic denitrification. Up to 1 μM Fe accumulated both in lDNT and hDNT (Fig. 3C and D). Concerning S^{2-}, it was not detected in hDNT but it reached 3 μM in lDNT treatment (Fig. 3C and D), which could result from a slight BSR activity. The ratio between BSR and denitrification rates tends to increase with higher electron donor availability (Laverman et al., 2012), as observed in lDNT compared to hDNT. Also, the fact that S^{2-} was detected in the lDNT experiment and not it the AMON experiment reinforced that NO_3^- reagent addition triggers a system disturbance that can lead to the activation of biological and/or physical processes.

Aiming to detect a potential chemodenitrification activity, NO_2^- concentration evolution in batch experiments containing deep sediment was compared with or without addition of external dissolved Fe^{2+} in the CHDN and FeCHD experiments, respectively. The total NO_2^- reduced after 4000 min incubation in the CHDN and FeCHDN experiments was approximately 30 and 40 %, respectively (Fig. 4A and B). Increased reactivity due to the addition of dissolved Fe^{2+} cannot be discarded, which is in accordance with previous chemodenitrification studies where Fe^{2+} addition increased NO_2^- reduction rates (Abu et al., 2024; Benaiges-Fernandez et al., 2020; Grabb et al., 2017; Margalef-Marti et al., 2020). Qualitative N_2O measurements showed a much higher accumulation in the CHDN and FeCHD compared to the lDNT and hDNT experiments (1-fold, Supporting Information S6). This suggested the

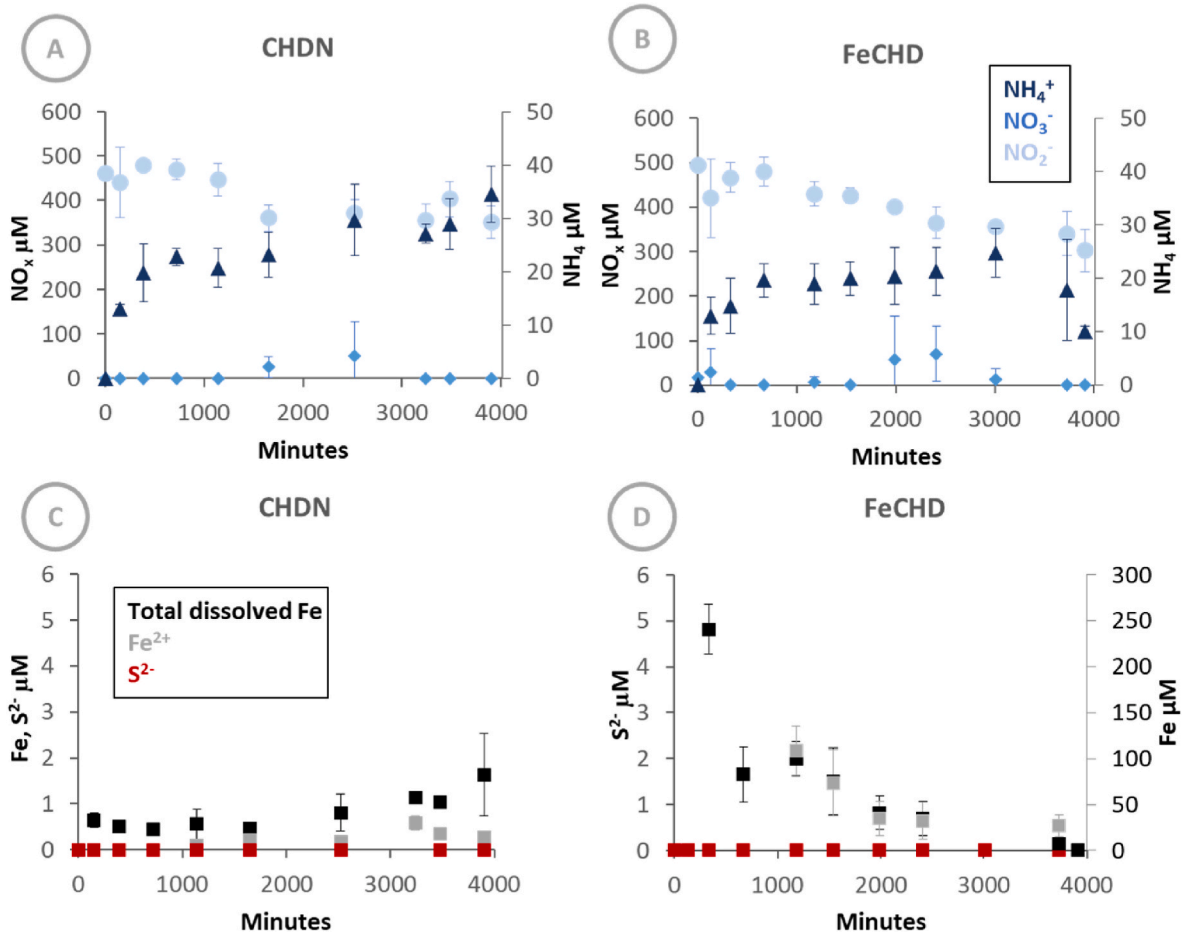

Fig. 4. Chemodenitrification experiments results. Plots A and B show the measured concentration of ammonium (dark blue triangles), nitrate (blue rhombus) and nitrite (light blue circle), while plots C and D show the measured concentration of sulphide (red squares), total dissolved iron (black squares) and dissolved ferrous iron (grey squares)). (For interpretation of the references to color in this figure legend, the reader is referred to the Web version of this article.)

occurrence of an abiotic reaction although presumably in combination with the biotic reduction. Accumulation of N_2O is usual in abiotic experiments since it is the final product in contrast to the biotic reduction where N_2 is the final product (Chen et al., 2018; Cooper et al., 2003; Robinson et al., 2021). However, the accumulated N_2O through chemodenitrification can be further reduced to N_2 by denitrifying microorganisms. On the other hand, similarly to what was observed in the lDNT and hDNT experiments, up to 35 and 25 µM NH_4^+ accumulated in CHDN and FeCHD, respectively, when starting the incubations. The reason of NH_4^+ accumulation in these experiments seems also desorption from sediment (Supporting information S4), which is activated after addition of NO_2^-.

Concerning Fe evolution, in the CHDN experiment it accumulated up to 1.5 µM (Fig. 4C), which is in the same range of that measured for the lDNT and hDNT experiments. In contrast, dissolved Fe^{2+} concentration decreased exponentially over time in the FeCHD experiment, where additional dissolved Fe^{2+} was injected (Fig. 4D). The fact that the measured Fe^{2+} concentration at the beginning of the experiment was below the expected (250 µM were measured while 500 µM were added) was attributed to the saturation limit of the method (250 µM). The observed decrease of concentration over time could be caused mainly by adsorption to sediment but also to oxidation, slightly increasing NO_2^- consumption in FeCHD with respect to CHDN. A previous study reported that biotically released Fe^{2+} is more reactive than synthetic Fe^{2+} (Benaiges-Fernandez et al., 2020). In this sense, the low increase on NO_2^- reactivity after dissolved Fe^{2+} injection could be due to the fact that intrinsic Fe^{2+} from the slurry is more reactive than the added synthetic one.

Reduction rates constants of NO_3^- or NO_2^- for all experiments were obtained using a pseudo-first order rate expression and the calculations are shown in Supporting Information S7. The reduction rate constants calculated considering the full incubation period for the lDNT, hDNT, FeCHD and CHDN experiments was 0.065, 0.018, 0.006 and 0.005 h^{-1}, respectively. However, when repeating calculations without considering the lag time, the rate constants increased to 0.091, 0.022, 0.007 and 0.005 h^{-1}, respectively. The highest constant rate was found for the lDNT experiment, followed by hDNT, FeCHD and finally CHDN.

A wide range of constant rates have been reported for chemodenitrification studies up to date, which range between 0.0001 and 6 h^{-1} (Table 2). The determined constant rates in our experiments are closer to the lowest ones, which coincides with the majority of published studies. Previous works at laboratory-scale underline that the parameters that mostly influence chemodenitrification rates are: (I) the NO_2^- to Fe^{2+} ratio (lower ratios trigger higher reactivity), (II) the solution ph (most of the studies have been performed at pH between 5.5 and 8.5), (III) the source of Fe^{2+} (biotically released or synthetically added), and particularly, (IV) if ferrous iron is found in the aqueous form or adsorbed or mineral or in a combination of various forms (Benaiges-Fernandez et al., 2020; Buchwald et al., 2016; Chen et al., 2020; Grabb et al., 2017; Jones et al., 2015; Robinson et al., 2021). The highest constant rates have been determined in experiments containing green rust (Grabb et al., 2017).

Table 2
Nitrite reduction constant rates. Comparative of reaction rate constants determined from batch experiments aiming to study the chemodenitrification.

Rate constant (h^{-1})	Initial NO_2^- (μM)	Initial dissolved Fe^{2+} (μM)	Environment	pH	Reference
0.005 (1st order)	500	11 (natural)	Gallocanta lake sediment	8.8	Present study
0.006 (1st order)	500	250 (synthetic)	Gallocanta lake sediment	8.8	Present study
0.0018 (1st order)	100	1000 (synthetic)	Walnut Creek sediment	7	Robinson et al. (2021)
0.0016 (1st order)	183	12000 (synthetic)	Artificial seawater	6.5	Grabb et al. (2017)
1-6 (1st order)	100–960	400-2300 (synthetic)	Artificial seawater + Green rust	6.5	Grabb et al. (2017)
0.0001-0.008 (1st order)	117–205	700-800 (synthetic)	Artificial seawater + Corundrum or Montmorillonite or Illite or Nontronite	6.5	Grabb et al. (2017)
0.03 (2nd order)	800	1200 (synthetic)	Artificial seawater + Ferrihydrite	8.2	Benaiges-Fernandez et al. (2020)
0.3 (2nd order)	800	1200 (biotic)	Artificial seawater + Ferrihydrite	8.2	Benaiges-Fernandez et al. (2020)
0.0007-0.1 (1st order)	200	600-8700 (synthetic)	HEPES buffer	7	Buchwald et al. (2016)
0.005-0.3 (1st order)	200	800-7900 (synthetic)	HEPES buffer + Goethite	7	Buchwald et al. (2016)
0.03-0.35 (1st order)	200	600-6300 (synthetic)	HEPES buffer	8	Buchwald et al. (2016)
0.05-1.7 (1st order)	200	1000-8100 (synthetic)	HEPES buffer + Goethite	8	Buchwald et al. (2016)
0.46 (1st order)	100	1000 (synthetic)	Bicarbonate buffer + Goethite	7	Robinson et al. (2021)
0.36 (1st order)	100	1000 (synthetic)	Bicarbonate buffer + Hematite	7	Robinson et al. (2021)
0.054-0.28 (1st order)	100	–	Bicarbonate buffer + Magnetite	7	Robinson et al. (2021)
0.01 (1st order)	100	1000 (synthetic)	Bicarbonate buffer + Maghemite	7	Robinson et al. (2021)
0.007 (1st order)	3000	9300 (synthetic)	MES-MOPS buffer	5.5	Chen et al. (2020)
0.01 (1st order)	3000	9300 (synthetic)	MES-MOPS buffer	6	Chen et al. (2020)
0.021 (1st order)	3000	9300 (synthetic)	MES-MOPS buffer	6.5	Chen et al. (2020)
0.041 (1st order)	3000	9300 (synthetic)	MES-MOPS buffer	7	Chen et al. (2020)
0.02 (1st order)	10000	10000 (synthetic)	PIPES buffer	–	Jones et al. (2015)
0.13 (1st order)	10000	10000 (synthetic)	PIPES buffer + Fe(III) (hydr)oxide	–	Jones et al. (2015)
0.005 (1st order) 3.4 (2nd order	1200	6000	Artificial groundwater	3.1	Abu et al. (2024)
0.012 (1st order) 3.4 (2nd order)	1200	6000	Artificial groundwater + siderite	5.5	Abu et al. (2024)

3.3. Isotopic fractionation during denitrification and chemodenitrification

An increase in the heavy isotopes in the remaining substrate was observed during NO_3^- reduction in the lDNT and hDNT experiments. The $\delta^{15}N$ values of NO_3^- increased from +4.5 to +9.7 ‰ and from +2.1 to +16.8 ‰, respectively, while the $\delta^{18}O$ values of NO_3^- increased from +18.8 to +23.3 ‰ and from +17.1 to +33.1 ‰, respectively (Fig. 5A and B). Because of the NO_3^- isotopic fractionation, the initially generated NO_2^- during denitrification in the lDNT and hDNT experiments presented a lower $\delta^{15}N$ compared to the initial NO_3^-. Subsequently, the $\delta^{15}N$ values of NO_2^- increased during the NO_3^- reduction from −18.6 to +12.7 ‰ and from −15.5 to −6.2 ‰, respectively (Fig. 5A and B).

The variations in the substrate isotopic composition during the lDNT and hDNT experiments led to $\varepsilon^{15}N_{NO3}$ of −8.5 and −15.1 ‰, respectively, and $\varepsilon^{18}O_{NO3}$ of −7.9 and −19.7 ‰, respectively (Fig. 5C and D). The resulting $\varepsilon^{15}N_{NO3}/\varepsilon^{18}O_{NO3}$ for the lDNT and hDNT experiments were 1.1 and 0.8, respectively. The obtained $\varepsilon^{15}N_{NO3}$ for lDNT and hDNT fell within the large range reported for the denitrification from −55 to −3‰ (Buchwald and Wankel, 2022; Granger et al., 2008). Most reported $\varepsilon^{15}N_{NO3}$ values for denitrification up to date correspond to heterotrophic activity studies. Nevertheless, two studies focusing on the autotrophic denitrification by pyrite oxidation found $\varepsilon^{15}N_{NO3}$ values from −15 to −28 ‰ (Torrentó et al., 2010, 2011). The obtained $\varepsilon^{15}N_{NO3}$ for hDNT (−15.1 ‰) fell within this range, but that obtained for lDNT was slightly lower (−8.5 ‰). As previously discussed, we assumed that NO_3^- reduction was mainly caused by oxidation of Fe^{2+}, and therefore by autotrophic bacteria activity because Gallocanta lake deep sediment do not contain significant organic matter amounts and because iron got remobilized during denitrification (Fig. 3C and D). In this sense, the $\varepsilon^{15}N_{NO3}$ values obtained for lDNT enlarge the range reported in the literature up to date for the autotrophic denitrification.

Three main factors can influence NO_3^- isotopic fractionation in closed conditions experiments: (I) the enzymes responsible for NO_3^- reduction, (II) the type of electron donor, and (III) the reduction rate, which is dependent on the ratio between NO_3^- and the electron donor (Asamoto et al., 2021; Granger et al., 2008; Wunderlich et al., 2012). The fact that lDNT and hDNT present different $\varepsilon^{15}N_{NO3}$ and $\varepsilon^{18}O_{NO3}$ values was likely due to the different NO_3^- reduction constant rates between the experiments (0.065 and 0.018 h^{-1}, respectively). A role from the microbial community enzymes and the type of electron donor should be discarded as both experiments presented the same initial conditions. Higher reduction rates are usually associated to less pronounced isotopic fractionation since higher kinetics mean lower free energy for the reaction and consequently, lower isotope discrimination along the transformation process (Mariotti et al., 1982). This is consistent with our observations of a higher $\varepsilon^{15}N_{NO3}$ for hDNT while a higher reduction constant rate was found for lDNT.

Concerning the CHDN and FeCHD experiments, an increase in the heavy isotopes was also observed in the remaining substrate during NO_2^- reduction. This leaded to a $\delta^{15}N$–NO_2^- increase from +1.8 to +5.6 ‰ and from +0.8 to +7.5 ‰, respectively (Fig. 5E and F). In contrast, the $\delta^{18}O$–NO_2^- did not variate significantly (Fig. 5E and F). The low variations on the $\delta^{18}O$–NO_2^- pointed the occurrence of equilibration between the $\delta^{18}O$–NO_2^- and the $\delta^{18}O$–H_2O as it has been previously observed in other NO_2^- isotopic studies (Granger and Wankel, 2016; Kool et al., 2007). For this reason, the $\delta^{18}O$–NO_2^- data, it is not further considered for discussion.

The calculated $\varepsilon^{15}N_{NO2}$ for the CHDN and FeCHD experiments were −6.8 and −12.3 ‰, respectively (Fig. 5G and H). These values are in the range of isotopic fractionation values previously reported for both the biotic (−2 to −45 ‰) and the abiotic (−3 to −26 ‰) NO_2^- reduction (Benaiges-Fernandez et al., 2020; Bryan et al., 1983; Buchwald et al., 2016; Grabb et al., 2017; Martin and Casciotti, 2016; Sebilo et al., 2019). As it is usually found for biotic experiments, more pronounced $\varepsilon^{15}N_{NO2}$ have been previously associated to lower chemodenitrification rates, while other parameters affecting the isotopic fractionation in chemodenitrification experiments are yet to be explored (Buchwald and Wankel, 2022; Grabb et al., 2017). It has to be noted that, considering the 95% confidence intervals, the determined $\varepsilon^{15}N_{NO2}$ for the CHDN and FeCHD experiments were not significantly different. However, we believe that slight differences cannot be discarded. The CHDN and FeCHD experiments showed similar NO_2^- reduction constant rates

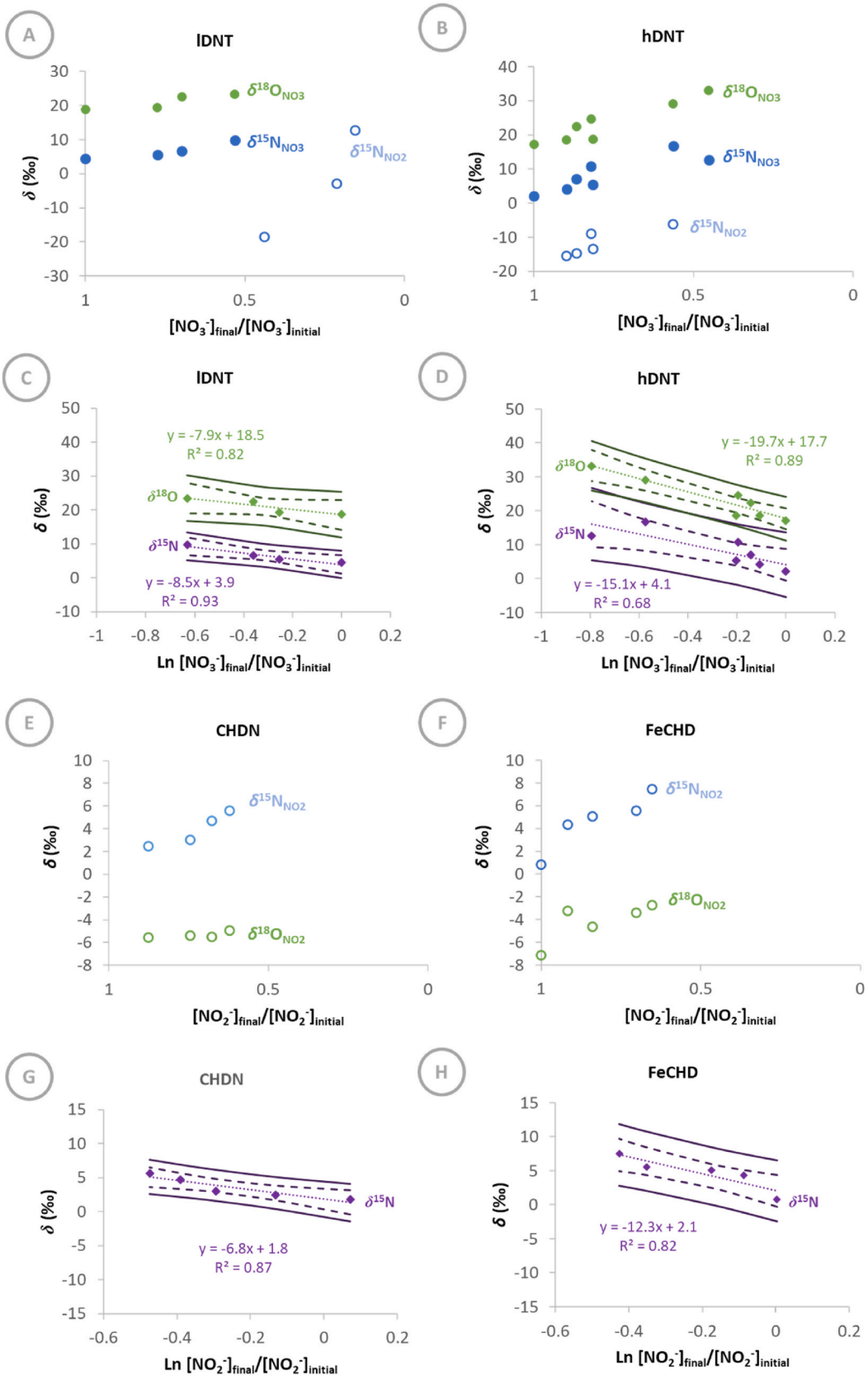

Fig. 5. Isotopic composition evolution and fractionation of N compounds in batch experiments. Measured $\delta^{15}N–NO_3^-$ and $\delta^{15}N–NO_2^-$ during NO_3^- reduction in lDNT and hDNT (A, B) and associated isotopic fractionation (C, D), and measured $\delta^{15}N–NO_2^-$ during NO_2^- reduction in CHDN and FeCHD (E, F) and associated isotopic fractionation (G, H). The $\varepsilon^{15}N$ and/or $\varepsilon^{18}O$ is obtained from the slope of the regression lines between the measured δ values and the natural logarithm of the substrate remaining fraction. The 95% confidence intervals are shown for plots C, D, G and H.

(0.005 and 0.006 h^{-1}, respectively) and therefore, they were not likely the cause of the different $\varepsilon^{15}N_{NO3}$ values obtained between the two types of experiments. Instead, the reason might be a different reaction mechanism or a different contribution of parallel mechanisms, e.g. a higher contribution of the chemodenitrification (abiotic) with respect to the denitrification (enzymatic) in FeCHD with respect to CHDN experiments. A comparison between the determined $\varepsilon^{15}N$ and the determined reduction rate constants for all experiment has been included in Supporting information S8. The CHDN and FeCHD experiments seem to follow a different pattern than the lDNT and hDNT experiments, reinforcing that different types of reduction mechanisms were involved in the NO_3^- compared to the NO_2^- containing experiments.

These results underline that in Gallocanta lake, NO_2^- generated during NO_3^- reduction could be further reduced by both the abiotic and biotic pathways. The fact that the chemodenitrification process is feasible in Gallocanta lake does not necessarily mean that it occurs continuously in this ecosystem. Firstly, NO_2^- and Fe^{2+} should be available on the same time and at the same sediment depth. In Gallocanta lake NO_2^- can only be present if denitrification and/or nitrification are active while Fe^{2+} content is relevant below surface sediment. The reason is that the bacterial sulfate reducing activity near the water-sediment interface leads to high S^{2-} accumulation and FeS precipitation. Further research should be done in other aquatic ecosystems with varying availability of organic carbon, sulfur, nitrogen and iron compounds to address under which kind of environments the chemodenitrification process can be more relevant.

4. Conclusions

When incubating NO_3^- with sediment (5–9 cm) from Gallocanta lake, denitrifying microorganisms were able to reduce it under autotrophic conditions (low organic carbon, high Fe^{2+}). A lag-time was observed before the start of NO_3^- reduction, pointing that Gallocanta lake does not contain NO_3^- permanently and consequently, denitrifying microorganisms are not always active. The determined $\varepsilon^{15}N_{NO3}$ for experiments containing low and high NO_3^- concentrations were −8.5 and −15.1 ‰, respectively, while $\varepsilon^{18}O_{NO3}$ were −7.9 and −19.7 ‰, respectively, which is consistent with denitrification. The more pronounced isotopic fractionation was found for the high NO_3^- concentration experiment and it was related to its lower reduction constant rates.

The geochemical and isotopic characterization of the experiments also allowed to highlight the feasibility of abiotic NO_2^- reduction in Gallocanta lake sediment (5–9 cm). The obtained $\varepsilon^{15}N_{NO2}$ were −6.8 ‰ and −12.3 ‰ for the experiments without and with additional Fe^{2+}, respectively. These values are in the range of those previously reported for the chemodenitrification but they overlap those reported for the biotic reduction. The slightly more pronounced $\varepsilon^{15}N_{NO2}$ values found for the experiments containing additional Fe^{2+} reinforced a higher contribution of the chemodenitrification with respect to the denitrification in these experiments.

This study showed the feasibility of chemodenitrification in Gallocanta lake, where anthropogenic inputs of N are low, and at a sediment depth between 5 and 9 cm Fe^{2+} is highly available while organic C is low. Further research should be conducted in other aquatic ecosystems with contrasting availability of organic carbon, sulfur, nitrogen and iron compounds to address under which environments the chemodenitrification process can be more relevant.

CRediT authorship contribution statement

Rosanna Margalef-Marti: Writing – original draft, Methodology, Data curation, Conceptualization. **Aubin Thibault De Chanvalon:** Writing – review & editing, Methodology, Data curation. **Pierre Anschutz:** Writing – review & editing, Methodology, Data curation. **David Amouroux:** Writing – review & editing, Methodology. **Mathieu Sebilo:** Writing – original draft, Methodology, Funding acquisition, Data curation, Conceptualization.

Declaration of competing interest

The authors declare that they have no known competing financial interests or personal relationships that could have appeared to influence the work reported in this paper.

Data availability

Data will be made available on request.

Acknowledgements

This work has been supported by Université de Pau et de Pays de l'Adour (UPPA) in the framework of the Energy Environment Solutions (E2S-UPPA) initiative of excellence (I-SITES, PIA France) for the Scientific Hub "Metals in Environmental Systems Microbiology (MESMic)" and by the french National Programme EC2CO (Hybige) in the context of the Fe/N-ICS project. We would like to thank the caretaker staff of Gallocanta Lake and INAGA for allowing us to collect the samples. We would also like to thank iEES (Paris) and MAiMA (Barcelona) groups for assistance on the isotopic analyses. Margalef-Marti, R. is grateful to the Spanish Government and University of Barcelona for the awarded Margarita Salas grant (Next Generation EU funds).

Appendix A. Supplementary data

Supplementary data to this article can be found online at https://doi.org/10.1016/j.chemosphere.2024.142292.

References

Abu, A., Carrey, R., Navarro-Ciurana, D., Margalef-Marti, R., Soler, A., Otero, N., Domènech, C., 2024. Isotopic and geochemical modeling approach to evaluate abiotic nitrite reduction by ferrous iron. Chem. Geol. 647, 121942 https://doi.org/10.1016/j.chemgeo.2024.121942.

Akunna, J.C., Bizeau, C., Moletta, R., 1993. Nitrate and nitrite reductions with anaerobic sludge using various carbon sources: glucose, glycerol, acetic acid, lactic acid and methanol. Water Res. 27, 1303–1312. https://doi.org/10.1016/0043-1354(93)90217-6.

Alonso López, J.A., Alonso López, J.C., Cantos, F.J., Bautista, L.M., 1990a. Spring crane *Grus grus* migration through Gallocanta, Spain. II. Timing and pattern of daily departures. Ardea 78, 379–388.

Alonso López, J.C., Alonso López, J.A., Cantos, F.J., Bautista, L.M., 1990b. Spring crane *Grus grus* migration through Gallocanta, Spain. I. Daily variations in migration volume. Ardea 78, 365–378.

Aravena, R., Robertson, W.D., 1998. Use of multiple isotope tracers to evaluate denitrification in ground water: study of nitrate from a large-flux septic system plume. Ground Water 36, 975–982.

Asamoto, C.K., Rempfert, K.R., Luu, V.H., Younkin, A.D., Kopf, S.H., 2021. Enzyme-specific coupling of oxygen and nitrogen isotope fractionation of the nap and nar nitrate reductases. Environ. Sci. Technol. 55, 5537–5546. https://doi.org/10.1021/acs.est.0c07816.

Badr, O., Probert, S.D., 1993. Environmental impacts of atmospheric nitrous oxide. Appl. Energy 44, 197–231. https://doi.org/10.1016/0306-2619(93)90018-K.

Benaiges-Fernandez, R., Offeddu, F.G., Margalef-Marti, R., Palau, J., Urmeneta, J., Carrey, R., Otero, N., Cama, J., 2020. Geochemical and isotopic study of abiotic nitrite reduction coupled to biologically produced Fe(II) oxidation in marine environments. Chemosphere 260, 127554. https://doi.org/10.1016/j.chemosphere.2020.127554.

Beusen, A.H.W., Bouwman, A.F., Van Beek, L.P.H., Mogollón, J.M., Middelburg, J.J., 2016. Global riverine N and P transport to ocean increased during the 20th century despite increased retention along the aquatic continuum. Biogeosciences 13, 2441–2451. https://doi.org/10.5194/bg-13-2441-2016.

Böttcher, J., Strebel, O., Voerkelius, S., Schmidt, H.L., 1990. Using isotope fractionation of nitrate-nitrogen and nitrate-oxygen for evaluation of microbial denitrification in a sandy aquifer. J. Hydrol. 114, 413–424. https://doi.org/10.1016/0022-1694(90)90068-9.

Bryan, B.A., Shearer, G., Skeeters, J.L., Kohl, D.H., 1983. Variable expression of the nitrogen isotope effect associated with denitrification of nitrite. J. Biol. Chem. 258, 8613–8617.

Buchwald, C., Grabb, K., Hansel, C.M., Wankel, S.D., 2016. Constraining the role of iron in environmental nitrogen transformations: dual stable isotope systematics of abiotic NO2-reduction by Fe(II) and its production of N2O. Geochem. Cosmochim. Acta 186, 1–12. https://doi.org/10.1016/j.gca.2016.04.041.

Buchwald, C., Wankel, S.D., 2022. Enzyme-catalyzed isotope equilibrium: a hypothesis to explain apparent N cycling phenomena in low oxygen environments. Mar. Chem. 244, 104140 https://doi.org/10.1016/j.marchem.2022.104140.
Burgin, A.J., Hamilton, S.K., 2007. Have we overemphasized the role of denitrification in aquatic ecosystems? A review of nitrate removal pathways. Front. Ecol. Environ. 5, 89–96. https://doi.org/10.1890/1540-9295(2007)5[89:HWOTRO]2.0.CO;2.
Carlson, H.K., Clark, I.C., Blazewicz, S.J., Iavarone, A.T., Coates, J.D., 2013. Fe(II) oxidation is an innate capability of nitrate-reducing bacteria that involves abiotic and biotic reactions. J. Bacteriol. 195, 3260–3268. https://doi.org/10.1128/JB.00058-13.
Castañeda, C., Gracia, F.J., Conesa, J.A., Latorre, B., 2020. Geomorphological control of habitat distribution in an intermittent shallow saline lake, Gallocanta Lake, NE Spain. Sci. Total Environ. 726 https://doi.org/10.1016/j.scitotenv.2020.138601.
Castañeda, C., Luna, E., Rabenhorst, M., 2017. Reducing conditions in soil of Gallocanta Lake, northeast Spain. Eur. J. Soil Sci. 68, 249–258. https://doi.org/10.1111/ejss.12407.
CHE, 2005. Confederación Hidrográfica del Ebro [WWW Document]. URL. https://www.chebro.es/. (Accessed 6 January 2022).
Chen, D., Liu, T., Li, X., Li, F., Luo, X., Wu, Y., Wang, Y., 2018. Biological and chemical processes of microbially mediated nitrate-reducing Fe(II) oxidation by *Pseudogulbenkiania* sp. strain 2002. Chem. Geol. 476, 59–69. https://doi.org/10.1016/j.chemgeo.2017.11.004.
Chen, D., Yuan, X., Zhao, W., Luo, X., Li, F., Liu, T., 2020. Chemodenitrification by Fe(II) and nitrite: pH effect, mineralization and kinetic modeling. Chem. Geol. 541, 119586 https://doi.org/10.1016/j.chemgeo.2020.119586.
Coby, A.J., Picardal, F.W., 2005. Inhibition of $NO3^-$ and NO_2^- reduction by microbial Fe (III) reduction : evidence of a reaction between NO_2^- and cell surface-bound Fe^{2+}. Appl. Environ. Microbiol. 71, 5267–5274. https://doi.org/10.1128/AEM.71.9.5267.
Cojean, A.N.Y., Lehmann, M.F., Robertson, E.K., Thamdrup, B., Zopfi, J., 2020. Controls of H_2S, Fe^{2+}, and Mn^{2+} on microbial NO_3^--reducing processes in sediments of an eutrophic lake. Front. Microbiol. 11.
Cooper, D.C., Picardal, F.W., Schimmelmann, A., Coby, A.J., 2003. Chemical and biological interactions during nitrate and goethite reduction by *Shewanella putrefaciens* 200. Appl. Environ. Microbiol. 69, 3517–3525. https://doi.org/10.1128/AEM.69.6.3517.
Corzo, A., Luzon, A., Mayayo, M.J., Bergeijk, S.A. van, Mata, P., Lomas, J.G. de, 2005. Carbonate mineralogy along a biogeochemical gradient in recent lacustrine sediments of Gallocanta Lake (Spain). Geomicrobiol. J. 22, 283–298. https://doi.org/10.1080/01490450500183654.
Denk, T.R.A., Mohn, J., Decock, C., Lewicka-Szczebak, D., Harris, E., Butterbach-Bahl, K., Kiese, R., Wolf, B., 2017. The nitrogen cycle: a review of isotope effects and isotope modeling approaches. Soil Biol. Biochem. 105, 121–137. https://doi.org/10.1016/j.soilbio.2016.11.015.
Dhakal, P., Matocha, C.J., Huggins, F.E., Vandiviere, M.M., 2013. Nitrite reactivity with magnetite. Environ. Sci. Technol. 47, 6206–6213. https://doi.org/10.1021/es304011w.
Fonselius, S.H., 1983. Determination of hydrogen sulphide, p. 73-80. In: Grasshoff, K., Ehrhardt, M., Kremling, K. (Eds.), Methods in Sea Water Analysis. Verlag Chemie, Weinheim, Germany.
Fukada, T., Hiscock, K.M., Dennis, P.F., Grischek, T., 2003. A dual isotope approach to identify denitrification in groundwater at a river-bank infiltration site. Water Res. 37, 3070–3078. https://doi.org/10.1016/S0043-1354(03)00176-3.
García-Robledo, E., Corzo, A., Papaspyrou, S., 2014. A fast and direct spectrophotometric method for the sequential determination of nitrate and nitrite at low concentrations in small volumes. Mar. Chem. 162, 30–36. https://doi.org/10.1016/j.marchem.2014.03.002.
Grabb, K.C., Buchwald, C., Hansel, C.M., Wankel, S.D., 2017. A dual nitrite isotopic investigation of chemodenitrification by mineral-associated Fe(II) and its production of nitrous oxide. Geochem. Cosmochim. Acta 196, 388–402. https://doi.org/10.1016/j.gca.2016.10.026.
Granger, J., Sigman, D.M., Lehmann, M.F., Tortell, P.D., 2008. Nitrogen and oxygen isotope fractionation during dissimilatory nitrate reduction by denitrifying bacteria. Limnol. Oceanogr. 53, 2533–2545. https://doi.org/10.4319/lo.2008.53.6.2533.
Granger, J., Wankel, S.D., 2016. Isotopic overprinting of nitrification on denitrification as a ubiquitous and unifying feature of environmental nitrogen cycling. Proc. Natl. Acad. Sci. USA 113, E6391–E6400. https://doi.org/10.1073/pnas.1601383113.
Greenberg, A.E., Clesceri, L.S., Eaton, A.D., 1992. Standard methods for examination of water and wastewater. Am. Public Health Assoc. Wash. DC.
Gruber, N., Galloway, J.N., 2008. An Earth-system perspective of the global nitrogen cycle. Nature 451, 293–296. https://doi.org/10.1038/nature06592.
Hargreaves, J.A., 1998. Nitrogen biogeochemistry of aquaculture ponds. Aquaculture 166, 181–212. https://doi.org/10.1016/S0044-8486(98)00298-1.
Hauck, R.D., 1984. Atmospheric nitrogen. Chemistry, nitrification, denitrification, and their interrelationships. In: Choudhry, G.G., Degens, E.T., Ehrhardt, M., Hauck, R.D., Kempe, S., Lion, L.W., Spitzy, A., Wangersky, P.J. (Eds.), The Natural Environment and the Biogeochemical Cycles, the Handbook of Environmental Chemistry. Springer, Berlin, Heidelberg, pp. 105–125. https://doi.org/10.1007/978-3-540-38829-6_5.
Jolly, I.D., McEwan, K.L., Holland, K.L., 2008. A review of groundwater-surface water interactions in arid/semi-arid wetlands and the consequences of salinity for wetland ecology. Ecohydrology (6). https://doi.org/10.1002/eco.
Jones, L.C., Peters, B., Pacheco, J.S.L., Casciotti, K.L., Fendorf, S., 2015. Stable isotopes and iron oxide mineral products as markers of chemodenitrification. Environ. Sci. Technol. 49, 3444–3452. https://doi.org/10.1021/es504862x.
Khan, I.A., Spalding, R.F., 2004. Enhanced in situ denitrification for a municipal well. Water Res. 38, 3382–3388. https://doi.org/10.1016/j.watres.2004.04.052.
Klueglein, N., Kappler, A., 2013. Abiotic oxidation of Fe(II) by reactive nitrogen species in cultures of the nitrate-reducing Fe(II) oxidizer *Acidovorax sp*. BoFeN1 - questioning the existence of enzymatic Fe(II) oxidation. Geobiology 11, 180–190. https://doi.org/10.1111/gbi.12019.
Knowles, R., 1982. Denitrification. Microbiol. Rev. 46, 43–70.
Kool, D.M., Wrage, N., Oenema, O., Dolfing, J., Groenigen, J.W.V., 2007. Oxygen exchange between (de)nitrification intermediates and H2O and its implications for source determination of NO_3^- and N_2O: a review. Rapid Commun. Mass Spectrom. 21, 3569–3578. https://doi.org/10.1002/rcm.3249.
Koroleff, F., 1976. Determination of nutrients. In: Grasshof, E., Kremling, E. (Eds.), Methods the Seawater Analysis. Verlag Chemie, Weinhein, New York.
Kraft, B., Strous, M., Tegetmeyer, H.E., 2011. Microbial nitrate respiration - genes, enzymes and environmental distribution. J. Biotechnol. 155, 104–117. https://doi.org/10.1016/j.jbiotec.2010.12.025.
Laverman, A.M., Pallud, C., Abell, J., Cappellen, P.V., 2012. Comparative survey of potential nitrate and sulfate reduction rates in aquatic sediments. Geochem. Cosmochim. Acta 77, 474–488. https://doi.org/10.1016/j.gca.2011.10.033.
Lin, J.T., Stewart, V., 1997. Nitrate Assimilation by Bacteria 39, vols. 1–30. https://doi.org/10.1016/S0065-2911(08)60014-4.
Liu, T., Chen, D., Luo, X., Li, X., Li, F., 2018. Microbially mediated nitrate-reducing Fe(II) oxidation: quantification of chemodenitrification and biological reactions. Geochem. Cosmochim. Acta. https://doi.org/10.1016/j.gca.2018.06.040.
Margalef-Marti, R., Carrey, R., Benito, J.A., Marti, V., Soler, A., Otero, N., 2020. Nitrate and nitrite reduction by ferrous iron minerals in polluted groundwater: isotopic characterization of batch experiments. Chem. Geol. 119691 https://doi.org/10.1016/j.chemgeo.2020.119691.
Margalef-Marti, R., Carrey, R., Merchán, D., Soler, A., Causapé, J., Otero, N., 2019. Feasibility of using rural waste products to increase the denitrification efficiency in a surface flow constructed wetland. J. Hydrol. 124035 https://doi.org/10.1016/j.jhydrol.2019.124035.
Margalef-Marti, R., Sebilo, M., Thibault De Chanvalon, A., Anschutz, P., Charbonnier, C., Lauga, B., Gonzalez-Alvarez, I., Tessier, E., Amouroux, D., 2023. Upside down sulphate dynamics in a saline inland lake. Sci. Rep. 13, 3032. https://doi.org/10.1038/s41598-022-27355-9.
Mariotti, A., Germon, J.C., Hubert, P., Kaiser, P., Letolle, R., Tardieux, A., Tardieux, P., 1981. Experimental determination of nitrogen kinetic isotope fractionation: some principles; illustration for the denitrification and nitrification processes. Plant Soil 62, 413–430. https://doi.org/10.1007/BF02374138.
Mariotti, A., Landreau, A., Simon, B., 1988. 15N isotope biogeochemistry and natural denitrification process in groundwater: application to the chalk aquifer of northern France. Geochem. Cosmochim. Acta 52, 1869–1878. https://doi.org/10.1016/0016-7037(88)90010-5.
Mariotti, A., Leclerc, A., Germon, J.C., 1982. Nitrogen isotope fractionation associated with the $NO_2^- \rightarrow N_2O$ step of denitrification in soils. Can. J. Soil Sci. 62, 227–241. https://doi.org/10.4141/cjss82-027.
Martin, T.S., Casciotti, K.L., 2016. Nitrogen and oxygen isotopic fractionation during microbial nitrite reduction. Limnol. Oceanogr. 61, 1134–1143. https://doi.org/10.1002/lno.10278.
Masclaux-Daubresse, C., Daniel-Vedele, F., Dechorgnat, J., Chardon, F., Gaufichon, L., Suzuki, A., 2010. Nitrogen uptake, assimilation and remobilization in plants: challenges for sustainable and productive agriculture. Ann. Bot. 105, 1141–1157. https://doi.org/10.1093/aob/mcq028.
McIlvin, M.R., Altabet, M.A., 2005. Chemical conversion of nitrate and nitrite to nitrous oxide for nitrogen and oxygen isotopic analysis in freshwater and seawater. Anal. Chem. 77, 5589–5595. https://doi.org/10.1021/ac050528s.
Rakshit, S., Matocha, C.J., Coyne, M.S., 2008. Nitrite reduction by siderite. Soil Sci. Soc. Am. J. 72, 1070. https://doi.org/10.2136/sssaj2007.0296.
Rakshit, S., Matocha, C.J., Coyne, M.S., Sarkar, D., 2016. Nitrite reduction by Fe(II) associated with kaolinite. Int. J. Environ. Sci. Technol. 13, 1329–1334. https://doi.org/10.1007/s13762-016-0971-x.
Rickard, D., Morse, J.W., 2005. Acid volatile sulfide (AVS). Mar. Chem. 97, 141–197. https://doi.org/10.1016/j.marchem.2005.08.004.
Robinson, T.C., Latta, D.E., Notini, L., Schilling, K.E., Scherer, M.M., 2021. Abiotic reduction of nitrite by Fe(II): a comparison of rates and N2O production. Environ. Sci. Process. Impacts 23, 1531–1541. https://doi.org/10.1039/D1EM00222H.
Ryabenko, E., Altabet, M. a, Wallace, D.W.R., 2009. Effect of chloride on the chemical conversion of nitrate to nitrous oxide for $\delta^{15}N$ analysis. Limnol Oceanogr. Methods 7, 545–552. https://doi.org/10.4319/lom.2009.7.545.
Sebilo, M., Aloisi, G., Mayer, B., Perrin, E., Vaury, V., Mothet, A., Laverman, A.M., 2019. Controls on the isotopic composition of nitrite ($\delta^{15}N$ and $\delta^{18}O$) during denitrification in freshwater sediments. Sci. Rep. 9, 1–14. https://doi.org/10.1038/s41598-019-54014-3.
Stookey, L.L., 1970. Ferrozine-A new spectrophotometric reagent for iron. Anal. Chem. 42, 779–781. https://doi.org/10.1021/ac60289a016.
Torrentó, C., Cama, J., Urmeneta, J., Otero, N., Soler, A., 2010. Denitrification of groundwater with pyrite and *Thiobacillus denitrificans*. Chem. Geol. 278, 80–91. https://doi.org/10.1016/j.chemgeo.2010.09.003.
Torrentó, C., Urmeneta, J., Otero, N., Soler, A., Viñas, M., Cama, J., 2011. Enhanced denitrification in groundwater and sediments from a nitrate-contaminated aquifer after addition of pyrite. Chem. Geol. 287, 90–101. https://doi.org/10.1016/j.chemgeo.2011.06.002.
Williams, W.D., 2002. Environmental threats to salt lakes and the likely status of inland saline ecosystems in 2025. Environ. Conserv. 29, 154–167. https://doi.org/10.1017/S0376892902000103.

Wunderlich, A., Meckenstock, R., Einsiedl, F., 2012. Effect of different carbon substrates on nitrate stable isotope fractionation during microbial denitrification. Environ. Sci. Technol. 46, 4861–4868. https://doi.org/10.1021/es204075b.

Zhang, L., Altabet, M.A., Wu, T., Hadas, O., 2007. Sensitive measurement of NH_4^+ N/N (δNH_4^+) at natural abundance levels in fresh and saltwaters. Anal. Chem. 79, 5297–5303. https://doi.org/10.1021/ac070106d.

Zhao, S., Jin, Q., Sheng, Y., Agrawal, A., Guo, D., Dong, H., 2020. Promotion of microbial oxidation of structural Fe(II) in nontronite by oxalate and NTA. Environ. Sci. Technol. 54, 13026–13035. https://doi.org/10.1021/acs.est.0c03702.

Zumft, W.G., 1997. Cell biology and molecular basis of denitrification. Microbiol. Mol. Biol. Rev. MMBR 61, 533–616.